Hindawi
Shock and Vibration
Volume 2019, Article ID 9383047, 14 pages
https://doi.org/10.1155/2019/9383047

Research Article

Two-Dimensional CFD Modeling of Hysteresis Behavior of MR Dampers

Pengfei Guo[1,2] **and Jing Xie**[2]

[1]*Key Lab of Structures Dynamic Behavior and Control of the Ministry of Education, Harbin Institute of Technology, Harbin, China*
[2]*School of Civil Engineering, Xi'an University of Architecture and Technology, Xi'an, China*

Correspondence should be addressed to Pengfei Guo; pengfei_guo@126.com

Received 8 November 2018; Revised 13 March 2019; Accepted 26 March 2019; Published 10 April 2019

Academic Editor: Nicola Caterino

So far, most previous studies on the nonlinear hysteresis analysis of ER/MR dampers have been limited to one-dimensional modeling techniques. A two-dimensional (2D) axisymmetric CFD model of MR dampers is developed in this work. The main advantage of the proposed 2D model of MR dampers lies in that it can be used to predict dynamic behavior of MR devices of arbitrary geometries. The compressibility of MR fluids is the main factor responsible for the hysteresis behavior of MR dampers, and it has been rarely investigated in previous multidimensional modeling of MR damper. In our model, the compressibility of MR fluids is taken into account by the two-dimensional constitutive model which is extended from a previous one-dimensional physical model. The model is solved by using the finite element method, and the movement of the piston is described by the moving mesh technique. The MR damper in a reference is simulated, and the model predictions show good agreement with the experimental data in the reference.

1. Introduction

Magnetorheological (MR) fluid damper shows great promises for semiactive vibration controls of civil structures [1–3], aerospace automobiles [4, 5], and aircraft [6–8] due to their advantages of mechanical simplicity, high dynamic range, low power requirements, large force capacity, and robustness.

The nonlinear hysteresis analysis of ER/MR dampers has been concentrated on one-dimensional modeling techniques because of their simplicity and easy physical interpretation, including quite maturing phenomenological modeling [9–12] and more recent rapid developing physical modeling [13–19]. Fruitful achievements have been made, which greatly deepens our understanding and broadens applications of ER/MR dampers. Notably, the hysteretic relationship between the piston velocity and damping force is found to be related to the compressibility and inertia of MR fluids [16, 17, 20, 21], while the hysteresis between the excitation current and damping force results from the hysteretic response of ferromagnetic materials [22].

Multidimensional analysis is receiving increasing attention because it is more accurate for general modeling of MR devices with arbitrary geometries. Using a generalized viscosity expressed in terms of a low degree polynomial function of the applied electric fields, Ursescu [23] simulated the ER flow in a channel with a prescribed inlet flow velocity and the free outlet. A two-dimensional (2D) computational fluid mechanics (CFD) model was constructed by Sahin et al. [24] for a MR valve having complex flow region. It showed apparent advantages of better agreements with the experimental data than the traditional 1D analytical model because the pressure drops in the elbows, expansions, entrance, and exit sections, which are neglected in the latter, are all considered in the CFD model. For MR valves with short orifice lengths, errors of analytical models become significantly large, especially at higher velocities, so a CFD model will be indispensable. Zhou and Bai [25] conducted a three-

dimensional (3D) numerical FEM analysis for MRF seal technology applied on a circular cooler. By defining the apparent viscosity as the ratio of the fluid's yield stress over the local shear rate, Gołdasz and Sapiński [26] studied a squeeze mode MR damper with a CFD model, and the well-known fact was confirmed that the compressive loads increase with the decreasing gap height. More recently, using the finite volume method on a two-dimensional moving grid, Syrakos et al. [27] successfully captured the hysteresis of a damper caused by the inertia of fluid under high-frequency loadings.

A multidimensional finite element model also helps us to better understand multiphysical behavior of MR dampers by including other physical aspects such as electromagnetic response. For example, Caterino et al. [28, 29] showed that the promptness of MR devices is almost exclusively dependent on the effectiveness of electromagnetic performances which directly determines the response time of MR dampers. Recently, Zheng et al. [22] established a more sophisticated multiphysics model which considered the magnetic, temperature, and flow fields, respectively, by the inverse Jiles–Atherton hysteresis model, conjugate heat transfer equations, and Navier–Stokes equations. With the piston movements described by a deformed mesh, Case et al. [30] developed a multiphysics finite element model for a small scale MR damper, and the coupling of the magnetic field with the flow field was achieved through a modified Bingham plastic material model which relates the fluid's dynamic viscosity to the intensity of the induced magnetic field. A similar work was conducted by Sternberg et al. [31] which couples a three-dimensional (3D) magnetostatic analysis with the flow analysis by using a bilinear Newtonian fluid with a field-dependent dynamic viscosity.

As mentioned above, the inertia and compressibility of fluids are the two main factors affecting the hysteresis behavior of MR dampers. However, the flow analyses in all the above 2D/3D models are still limited to the inertia effect of fluid, with the main differences lying in the different modifications or regulations of the 2D/3D Bingham model. So far, the 2D modeling of the hysteresis of ER/MR dampers arisen from the compressibility of fluids has not been reported yet, and this motivates the present work.

2. 2D Moving Mesh Finite Element Modeling of Hysteresis of MR Dampers

2.1. Problem Definition and Governing Equations. The layout of a MR damper is shown in Figure 1. A piston of radius R_p, with a shaft of radius R_s, at its center, divides the damper into the top and bottom chambers. Movement of the piston causes MR fluids to flow through the annular gap between the house cylinder and the piston. The working gap has a width of g and effective length of L. Because this work focuses on the flow analysis, the whole space filled with MR fluid between the piston and the house cylinder is the physical domain of the finite element model to be constructed later, with the magnetic field related geometries such as coils omitted. The damper has a stroke of s_0, and a two-dimensional cylindrical coordinate system is adopted as shown in Figure 1.

2.2. Conservation of Momentum. The flow of MR fluids in MR dampers is governed by the well-known Navier–Stokes equations:

$$\rho\left(\frac{\partial v_i}{\partial t} + v_j\frac{\partial v_i}{\partial x_j}\right) = \sigma_{ij,j} + \rho b_i, \quad i = 1, 3, \tag{1}$$

where i and j are tensor indexes, $x_1 = r$ and $x_3 = z$ in cylindrical coordinate systems, v_i is the flow velocity component along x_i-coordinate, b_i is the body force along coordinate x_i and will be neglected in this study, σ_{ij} is the total stress tensor, $(\sigma)_{ij,j}$ is the divergence operator in the cylindrical coordinate system, and ρ is the density of MR fluids.

2.3. Conservation of Mass. The effect of the compressibility of MR fluid, which will be taken into account in the constitutive model, is assumed to be negligible on the fluid density. Then, the conservation of mass is expressed simply by the vanishing divergence of the flow velocity:

$$v_{i,i} = 0, \quad i = 1, 3. \tag{2}$$

2.4. A 2D Constitutive Model Inspired from 1D Physical Model. Problems of fluid viscoelasticity is notorious for being extremely difficult and challenging because of numerical difficulties such as the advective nature of the constitutive equations and the interaction of multiple discrete unknown fields (viscoelastic stress, velocity, and pressure) [32].

In the case where the displacement gradients of the flow are infinitesimal, the time derivatives on the stress and strain tensors are simply the common partial derivative with respect to the time ($\partial/\partial t$). When the displacement gradients of the flow are large, the time derivatives, $\partial/\partial t$, must be replaced with the convected derivatives of the stress and strain tensors, also known as contravariant convected time derivative [33]. Because the preyield MR fluid behaves like a rigid solid, the displacement gradients are infinitesimal. And for simplicity, we assume that the stress variation with time for the whole MR fluid flow, including both the pre- and postyield zones, can still be approximated by a common partial time derivative.

1D phenomenal or physical models [15, 16, 20] have been successfully used to predict the hysteresis of MR dampers, so it is naturally to expect a 2D extension from them. Guo et al. [15] developed a simple physical model as shown in Figure 2, which can be mathematically described by

$$\dot{\varepsilon} = \dot{\varepsilon}_k + \dot{\varepsilon}_\eta = \frac{\dot{s}}{k} + \frac{s}{\eta}, \tag{3}$$

where $\dot{\varepsilon}$ is the total strain rate, $\dot{\varepsilon}_k$ and $\dot{\varepsilon}_\eta$ are the elastic and viscous parts of the total strain rate, k is the stiffness of the spring representing the compressibility of MR fluid,

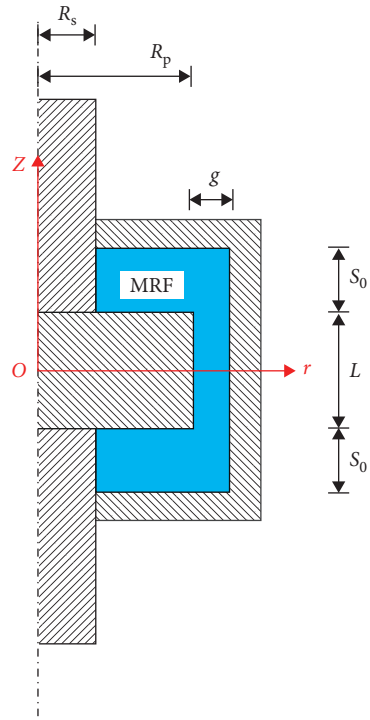

Figure 1: Typical configuration of a MR damper.

and η is the viscosity characterizing the quasistatic model of MR dampers.

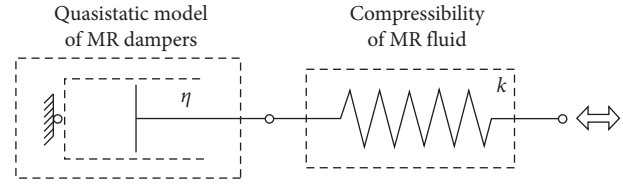

Figure 2: A physical model of MR dampers.

Equation (3) can be rewritten as

$$\dot{s} = k\dot{\varepsilon} - \frac{k}{\eta}s. \tag{4}$$

Inspired from the above 1D constitutive for the physical modeling of hysteresis of MR dampers, the following 2D extension constitutive model in terms of the symmetric viscous stress tensor is proposed:

$$\frac{\partial \tau_{ij}}{\partial t} = KD_{ij} - \frac{K}{\eta}\tau_{ij}, \quad i, j = 1, 3, \tag{5}$$

where D_{ij} is the strain rate tensor defined by $D_{ij} = v_{i,j} + v_{j,i}$, τ_{ij} is the symmetric viscous tensor ($\tau_{ij} = \tau_{ji}$) and K is the material parameter related to the compressibility of MR fluids. The viscosity of the modified Bingham model, η, is defined to be dependent on the yield stress of MR fluid, i.e.,

$$\eta = \begin{cases} \dfrac{\tau_y}{|D_{ij}|}\left(1 - \exp\left(-m|D_{ij}|\right)\right), & i, j = 1, 3, \text{ MR fluids in the working gap,} \\ \alpha, & \text{MR fluids in the chambers,} \end{cases} \tag{6}$$

where α is a small positive real number to avoid error of division by zero and it is set to 10^{-8}; the shear rate magnitude $|D_{ij}|$ is defined by

$$|D_{ij}| = \sqrt{\frac{1}{2}D_{ij}D_{ij}}, \quad i, j = 1, 3. \tag{7}$$

The simplicity of the constitutive model (equation (5)) comes at the cost of use of a nonobjective derivative, and the validation of this constitutive model will be demonstrated later by its comparison with experimental data.

Then, the total stress tensor in equation (1) is

$$\sigma_{ij} = 2\eta_N D_{ij} - p\delta_{ij} + \tau_{ij}, \quad i, j = 1, 3, \tag{8}$$

where η_N is the postyield viscosity and δ_{ij} is the identity tensor.

2.5. Moving Mesh. Moving mesh technique is required to include the arbitrary motion of the piston. Because the ratio of width to length of the working gap size is extremely large, mesh movement should be carefully handled. Linear interpolating moving equations are adopted in this work to avoid severe element distortions, thus improving the converging ability of the finite element model. Because the movement of the piston involves only the movement in z-direction, the interpolation is performed only in z-coordinates, with r-coordinates held constant.

2.5.1. Movement of the Piston. The displacement of the piston (z_p) is

$$z_p = z_0 \sin(2\pi f t), \tag{9}$$

where z_0 is the amplitude of sinusoidal piston displacement, f is the excitation frequency, and t is time.

2.5.2. Mesh of the Gap Domain. The mesh of the working gap moves as a rigid translation in z-direction:

$$z_{gap} = z_p, \quad z_{gap} \in \text{gap domain}, \tag{10}$$

where z_{gap} is the Euler coordinates of the material points (fluid particles) in the gap domain.

2.5.3. Mesh of Chamber. The mesh of the chambers is stretched or compressed, which can be described by the following linear interpolating functions:

$$z = \begin{cases} z_{\text{top}}, & z \in \text{top chamber domain}, \\ z_{\text{bot}}, & z \in \text{bottom chamber domain}, \end{cases}$$

$$z_{\text{top}} = z_{\text{p}} \frac{Z - Z_{\text{top0}}}{Z_{\text{top1}} - Z_{\text{top0}}}, \tag{11}$$

$$z_{\text{bot}} = z_{\text{p}} \frac{Z - Z_{\text{bot0}}}{Z_{\text{bot1}} - Z_{\text{bot0}}},$$

where z is the Euler coordinates of the material points occupying the chambers, Z_{top1} and Z_{bot1} are the Lagrangian coordinates at which the node displacements equal to the piston displacement, and Z_{top0} and Z_{bot0} are the Lagrangian coordinates at which the node displacement are zeros. For the coordinate system in Figure 1, these key coordinates are $Z_{\text{top1}} = L/2, Z_{\text{bot1}} = -L/2, Z_{\text{top0}} = (s_0 + L/2)$, and $Z_{\text{bot0}} = -(s_0 + L/2)$.

2.6. Boundary Conditions. The Dirichlet boundary conditions (BCs) for the flow velocity are shown in Figure 3. And natural (i.e., zero flux) BCs are implemented for the viscous tensor and pressure as

$$\frac{\partial \tau_{ij}}{\partial n} = 0, \qquad \frac{\partial p}{\partial n} = 0, \tag{12}$$

where n is the outward normal vector of the boundary.

2.7. Initial Conditions. The initial values of viscous stress, the pressure, and the flow velocity are all assumed to be zeros.

2.8. Evaluation of Damping Force. The damping force, F, can be calculated by integrating the pressure along the piston boundaries as

$$F = \left(\int_{z=L/2} p 2\pi r \, dr - \int_{z=-L/2} p 2\pi r \, dr \right) A_{\text{p}}, \tag{13}$$

where A_{p} is the effective area of the piston, $A_{\text{p}} = \pi(R_{\text{p}}^2 - R_{\text{s}}^2)$.

3. Implementation of the Proposed Model in COMSOL Multiphysics

The model equations are implemented in COMSOL Multiphysics software. The constitutive equation, the mass conservation equation, and the momentum conservation equation are implemented, respectively, by using three built-in PDE modules which have the following general form PDE:

$$e_{\text{a}} \frac{\partial^2 \mathbf{u}}{\partial t^2} + d_{\text{a}} \frac{\partial \mathbf{u}}{\partial t} + \nabla \cdot \boldsymbol{\Gamma} = \mathbf{f}, \tag{14}$$

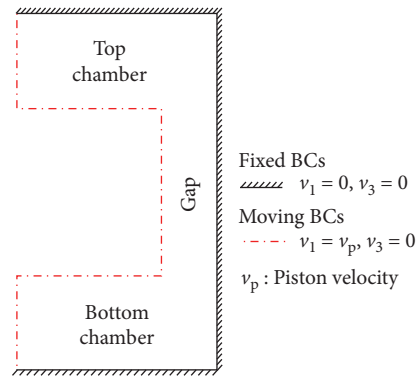

Figure 3: Boundary conditions for flow velocity.

where $\mathbf{u}$ is the vector of variables to be solved, $\boldsymbol{\Gamma}$ is the conservative flux vector, $\mathbf{f}$ is the source term vector, e_{a} is the mass coefficient matrix, and d_{a} is the damping coefficient matrix. For the model of MR dampers in this work, a total of 7 variables need to be defined in COMSOL, i.e., two velocity components (u and w), four shear stress components (tau11, tau13, tau22, and tau33), and a pressure field (p). These three PDE modules share the same fluid domain. For the convenience of implementation, we defined several auxiliary variables as listed in Table 1.

Detailed implementation of the proposed model is given in the following sections.

3.1. PDE Module 1 in COMSOL: Constitutive Equation (Variables: tau11, tau13, tau22, and tau33). In COMSOL, tensors are implemented as matrixes or vectors. The constitutive equation was implemented in the source term $\mathbf{f}$ as a fourth-order vector, i.e.,

$$\mathbf{f} = \begin{bmatrix} K * \text{D11} - (K/\text{eta}) * \text{tau11} \\ K * \text{D13} - (K/\text{eta}) * \text{tau13} \\ K * \text{D22} - (K/\text{eta}) * \text{tau22} \\ K * \text{D33} - (K/\text{eta}) * \text{tau33} \end{bmatrix}, \tag{15}$$

where the domain-dependent auxiliary variable, eta, is the COMSOL implementation of equation (6). The damping coefficient matrix, d_{a}, is the fourth-order identity matrix. The conservative flux $\boldsymbol{\Gamma}$ is a zero vector and the mass coefficient, e_{a}, is a zero square matrix. The whole input of the constitutive equation in COMSOL is shown in Figure 4.

3.2. PDE Module 2 in COMSOL: Mass Conservation Equation (Variable: p). The mass conservation equation is implemented in the source term of the general form PDE as $\mathbf{f}$ = vdiv, where the auxiliary variable, vdiv, is defined in Table 1. All the coefficient matrices are zero matrices. The complete input of the mass conservation equation in COMSOL is shown in Figure 5.

3.3. PDE Module 3 in COMSOL: Momentum Conservation Equation (Variables: u and w). The Cauchy stress is implemented in the conservative flux vector as

Table 1: Auxiliary variables defined in COMSOL for implementation convenience.

Physical meaning	Name	Expression in COMSOL
Shear rate	D11	$2 * ur$
	D13	$uz + wr$
	D22	$2 * u/r$
	D33	$2 * \mathrm{wz}$
Magnitude of shear rate	sr	Sqrt $(0.5 * 4 * (u/r)^2 + 2 * (uz + wr)^2 + 4 * (wz)^2 + \mathrm{eps})$
Total stress	Sigma11	etan * D11 + tau11-p
	Sigma13	etan * D13 + tau13
	Sigma22	etan * D22 + tau22-p
	Sigma33	etan * D33 + tau33-p
Divergence of velocity	vdiv	$u/r + ur + wz$

Note. According to the expression conventions of COMSOL, the spatial derivative of a variable, for example, $\partial u/\partial r$, is represented by u/r. The postyield viscosity implemented in COMSOL, etan, is 1.5 Pa·s.

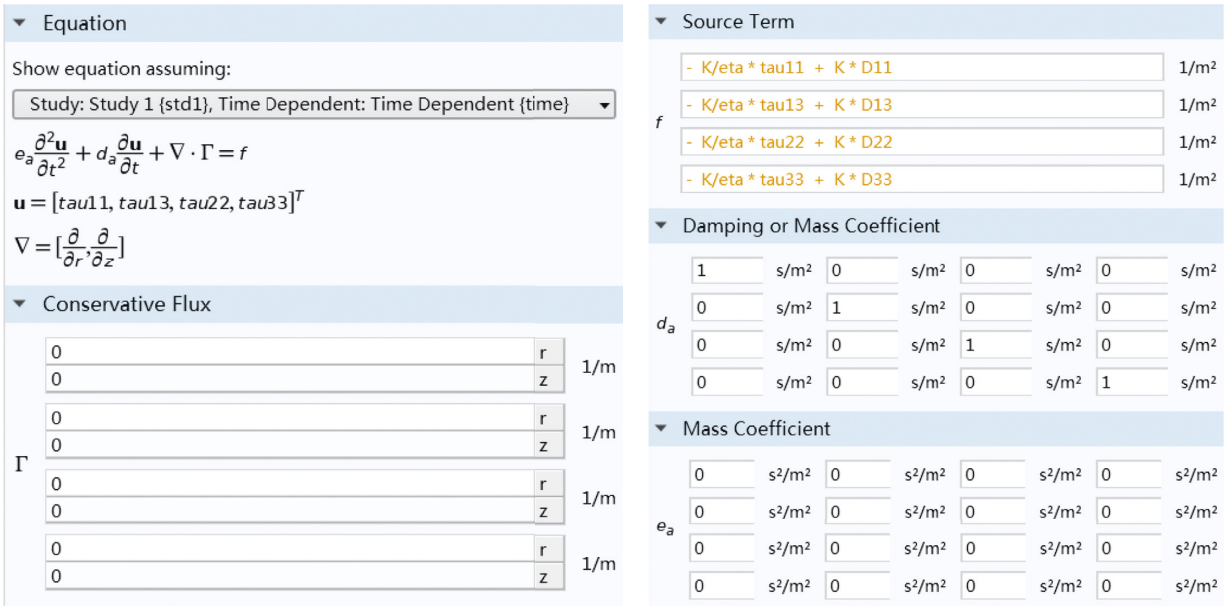

(a) (b)

Figure 4: Input of constitutive equation in COMSOL. (a) Conservative flux term. (b) Source term, damping coefficient matrix, and mass coefficient matrix.

$$\mathbf{\Gamma} = \begin{bmatrix} -\mathrm{sigma11} \\ -\mathrm{sigma13} \\ -\mathrm{sigma13} \\ -\mathrm{sigma33} \end{bmatrix}. \tag{16}$$

The convective part of the time derivative of velocity is included in the source term as

$$\mathbf{f} = \begin{bmatrix} -\mathrm{rho} * (\mathrm{u} * \mathrm{ur} + \mathrm{w} * \mathrm{uz}) + (\mathrm{sigma11} - \mathrm{sigma22})/\mathrm{r} \\ -\mathrm{rho} * (\mathrm{u} * \mathrm{wr} + \mathrm{w} * \mathrm{wz}) + (\mathrm{sigma13})/\mathrm{r} \end{bmatrix}. \tag{17}$$

Apparently, the damping coefficient matrix is simply a second-order unit matrix. The complete input of the momentum conservation equation in COMSOL is shown in Figure 6.

3.4. Moving Mesh (ALE) Module: Motion Equation of Mesh. The mesh motion can be readily implemented in COMSOL by just prescribing the mesh motion equation in the built-in moving mesh (ALE) module, as shown in Figure 7.

3.5. Solver Configuration. The built-in implicit backward differentiation formula (BDF) solver in COMSOL is used to solve the equation system for the model. The absolute solver tolerance is set to 1×10^{-5}, and the maximum of iterations is raised up to 1×10^3. All other solver configurations use default settings.

4. Validation of the Proposed Model

4.1. Mesh Sensitivity Analysis. Before validating the FEM model by using experimental data, it is necessary to study the

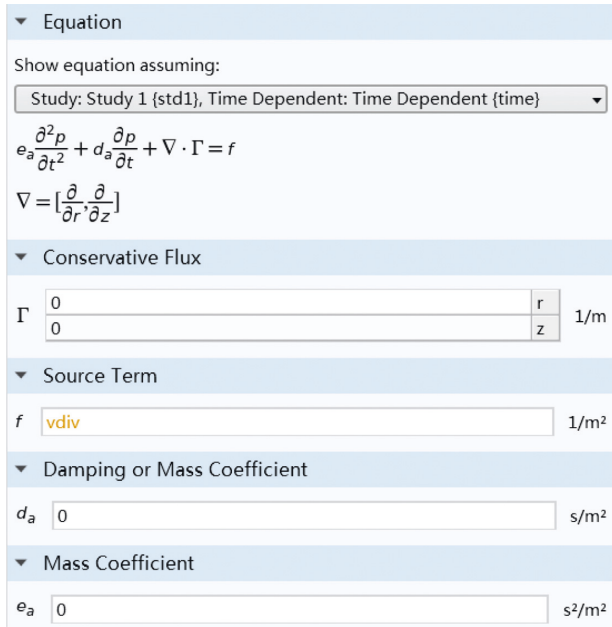

Figure 5: Input of mass conservation equation in COMSOL.

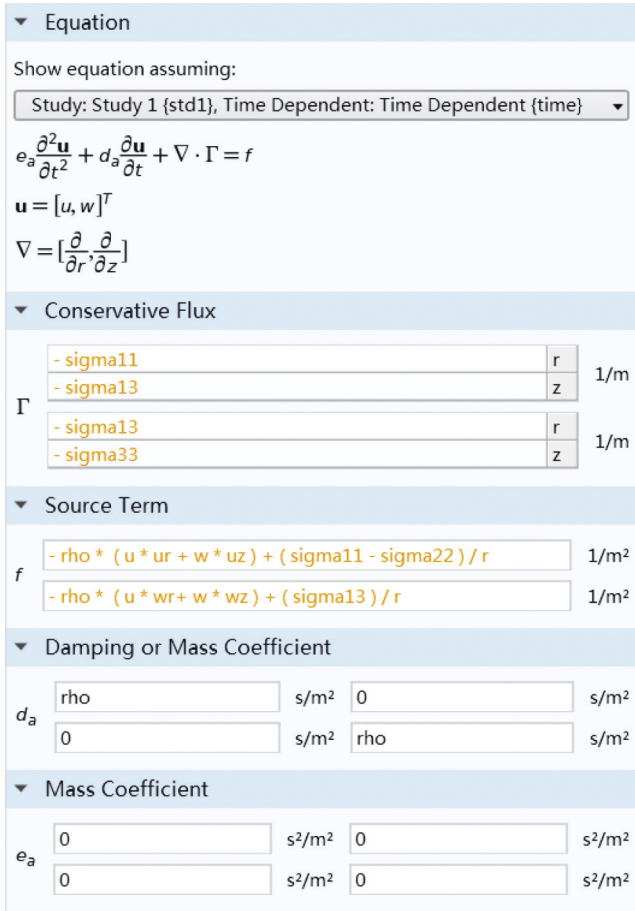

Figure 6: Input of momentum conservation equation in COMSOL.

effect of mesh sensitivity of the model results. Three refinement levels, i.e., coarse, normal, and fine meshes with 13656, 50698, and 127018 degrees of freedom (DOFs), respectively (Figure 8), were used to simulate the performance of the MR damper under a medium-frequency sinusoidal displacement excitation (2.54 cm, 0.1 Hz, 2 A). The

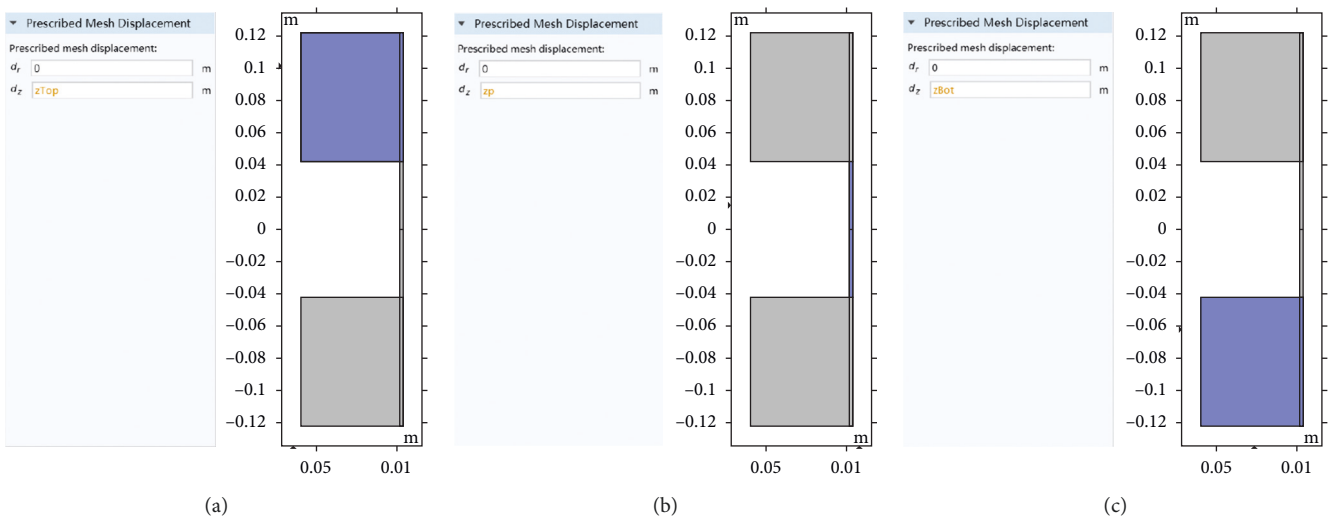

Figure 7: Input of mesh motion equation in COMSOL. (a) Top chamber. (b) Working gap. (c) Bottom chamber.

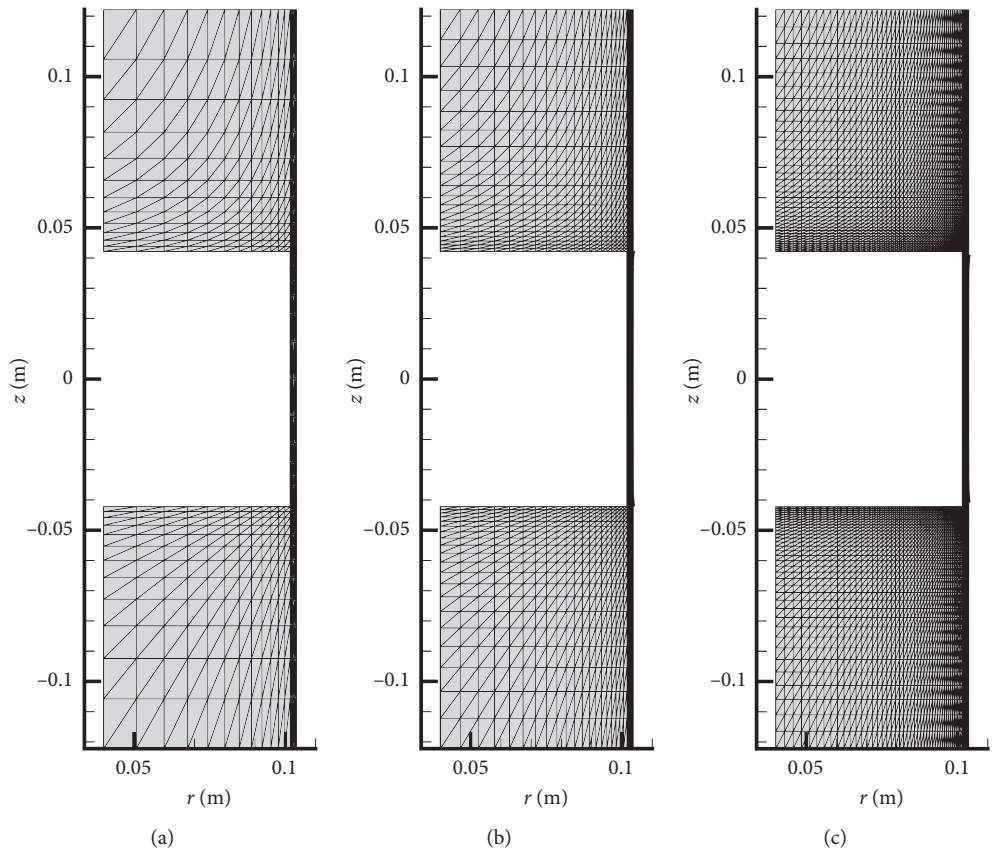

Figure 8: FEM meshes with different refinement levels. (a) Coarse mesh (13656 DOFs). (b) Normal mesh (50698 DOFs). (c) Fine mesh (127018 DOFs).

differently refined meshes are shown in Figure 8, with their close-up views presented in Figure 9.

As shown in Figure 10, the difference between the model results is negligible, and we will choose the normal mesh in the following validation of the model. It took about 8 hours to solve the model with the fine mesh on a personal computer (i5 CPU, 4G RAM), while the models with coarse or normal meshes only took less than 1 hour.

4.2. Experimental Validation. The experimental data of the MR damper in the study by Yang [34] under different

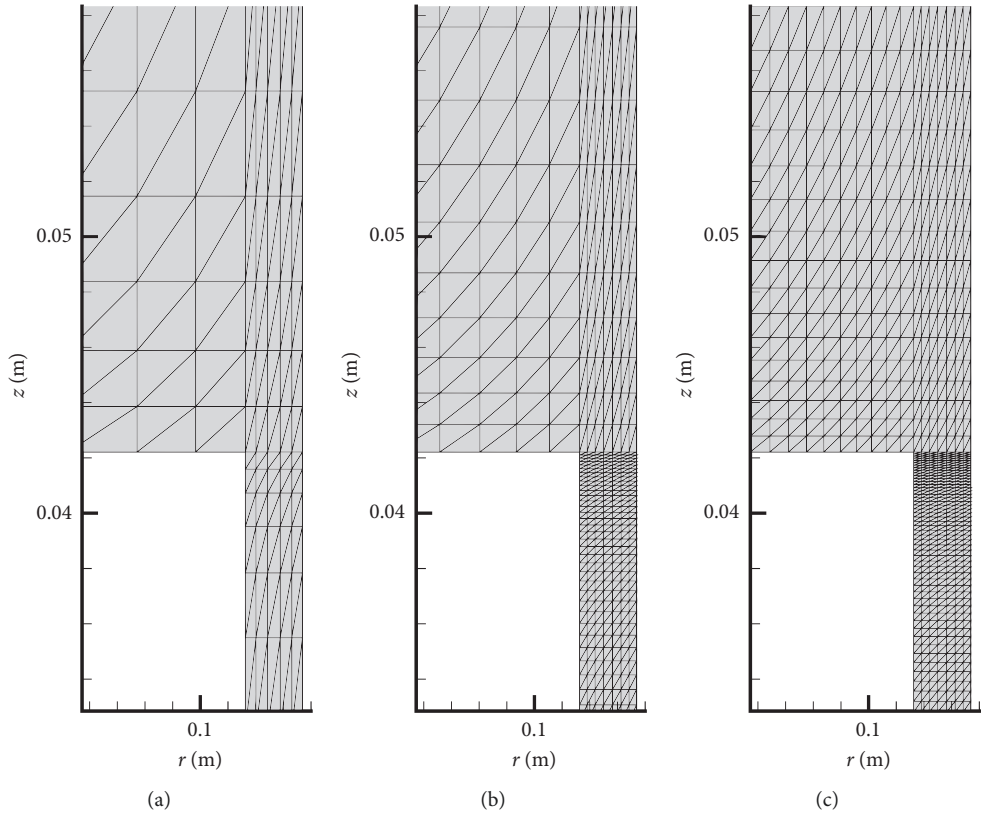

Figure 9: Close view of FEM meshes. (a) Coarse mesh. (b) Normal mesh. (c) Fine mesh.

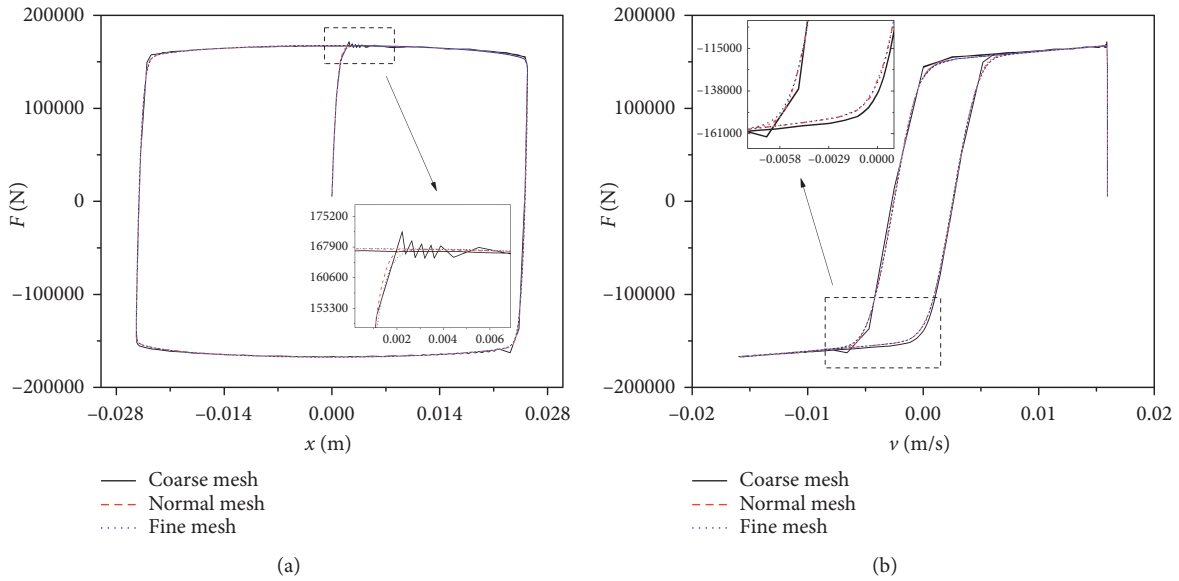

Figure 10: Effect of mesh refinement on FEM results.

operating conditions (exciting current: 0.25 A, 2 A; amplitude/frequency: 5.08 cm/0.05 Hz, 2.54 cm/0.1 Hz, 1.27 cm/0.2 Hz, 0.254 cm/1 Hz) will be used to validate the proposed model. The main structural parameters of the damper are listed in Table 2. By fitting the experimental data in the case of 5.08 cm, 0.05 Hz, 0.25 A, the material constants, K and m, are identified to be 0.2×10^4 and 0.25, respectively. Then, the performances of the damper in the other seven cases are predicted with this set of values. As shown in Figures 11–14, the model predictions are in good agreement with the experimental data, so the proposed model is reliable.

Table 2: The configuration of the damper in Yang' study [34].

Variable	Physical meaning	Value
G	Gap width	2.057 mm
S_0	Stroke	80 mm
R_p	Piston radius	101.63 mm
R_s	Piston shaft radius	40 mm
L	Effective axial pole length	84.428 mm
η_N	Postyield viscosity of MR fluid	1.5 Pa·s

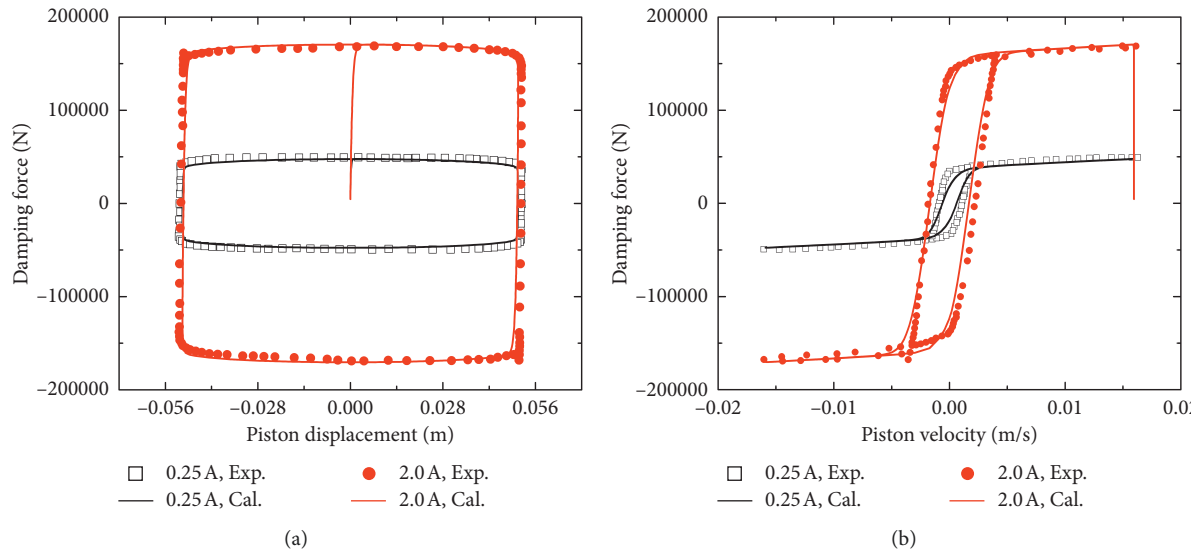

Figure 11: Model predictions (lines) and experimental data (Yang [34]) of hysteretic behavior of MR dampers under sinusoidal displacement excitations of 5.08 cm, 0.05 Hz. (a) Displacement-force hysteresis. (b) Velocity-force hysteresis.

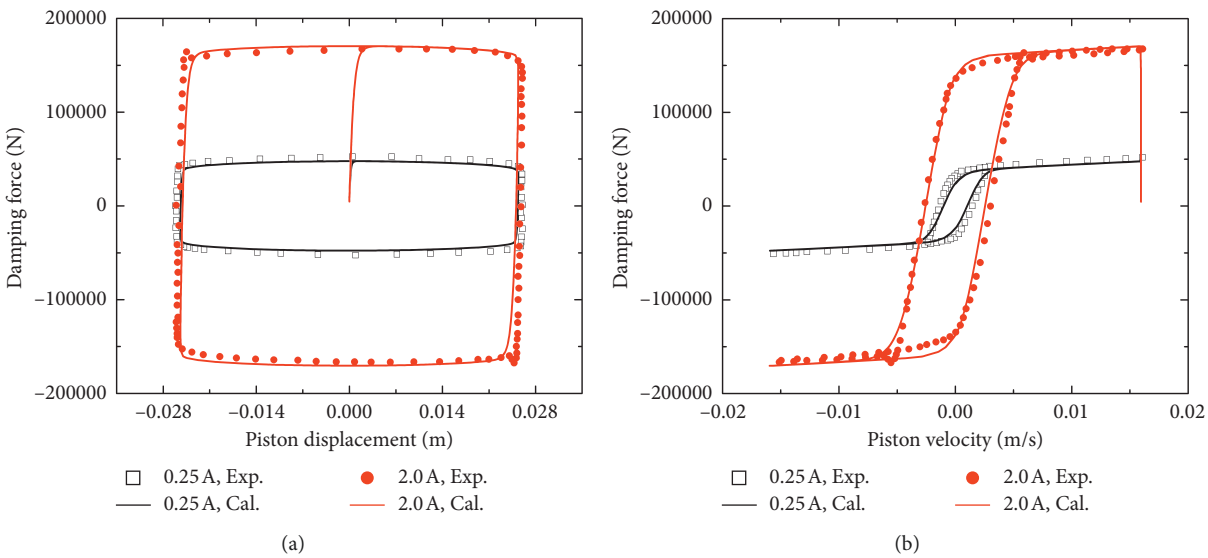

Figure 12: Model predictions (lines) and experimental data (Yang [34]) of hysteretic behavior of MR dampers under sinusoidal displacement excitations of 2.54 cm, 0.1 Hz. (a) Displacement-force hysteresis. (b) Velocity-force hysteresis.

Due to an applied magnetic field, the MR fluid in the working gap consists of chain structures, leading to a very large preyield viscosity (i.e., the shear yield strength). This rheology character of MR fluids gives rise to the stick-slip friction-like response of the damping force with respect to the piston velocity. When a MR damper works in the preyield zone, for example, when the piston slowly starts moving from the rest, the pressure in the pressurized

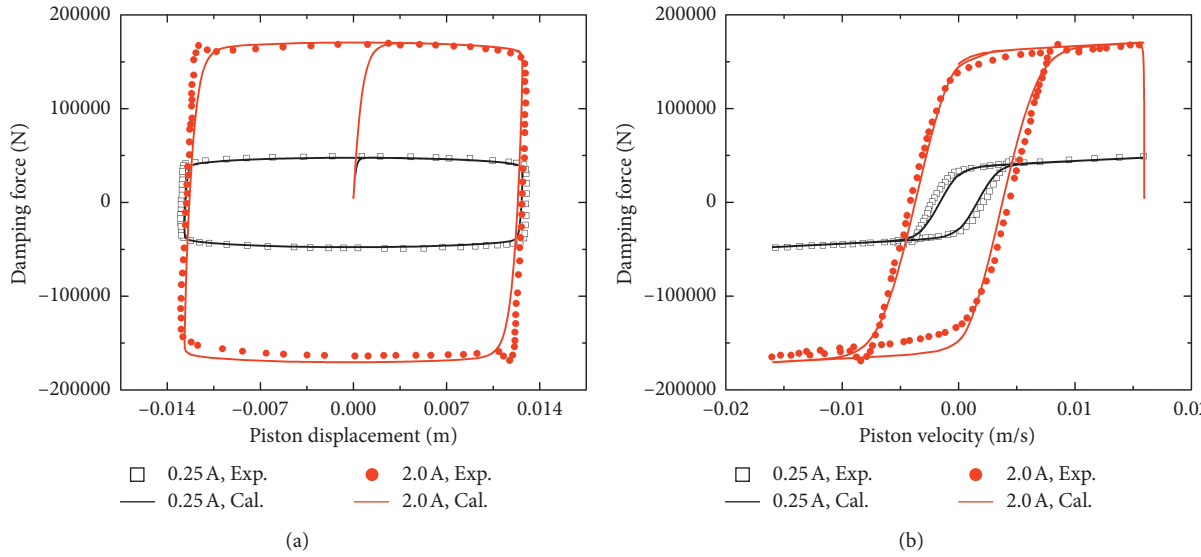

Figure 13: Model predictions (lines) and experimental data (Yang [34]) of hysteretic behavior of MR dampers under sinusoidal displacement excitations of 1.27 cm, 0.2 Hz. (a) Displacement-force hysteresis. (b) Velocity-force hysteresis.

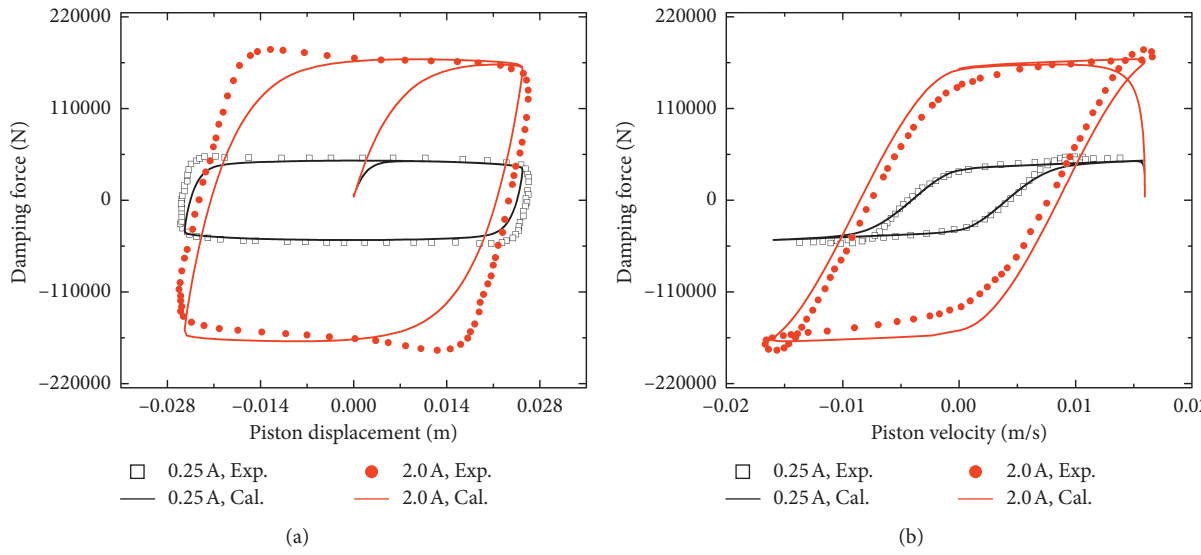

Figure 14: Model predictions (lines) and experimental data (Yang [34]) of hysteretic behavior of MR dampers under sinusoidal displacement excitations of 0.254 cm, 1 Hz. (a) Displacement-force hysteresis. (b) Velocity-force hysteresis.

chamber gradually grows due to the compressibility of MR fluid in chamber. Then, it accumulates constantly until it becomes large enough to overcome the yield strength and makes the fluid in the gap start to flow. The change in the damping force lags behind the change in the piston velocity, due to the compressibility of MR fluid. Thus, a hysteresis between the damping force and the piston velocity will be observed when a MR damper is working in the preyield zone, even if the pressure in the pressurized chamber is relatively low.

While keeping the maximum piston velocity unchanged (about 0.015 m/s as shown in Figures 11–14), the excitation amplitude decreases with increasing excitation frequency. Accordingly, the compression or the pressure accumulation of the fluid in the pressurized chamber is small under high-frequency excitations, and the MR damper works mainly at in preyield zone. For this reason, it is indeed observed in Figures 11–14 that the hysteresis of the damping force with respect to the piston velocity becomes apparently wider with increasing excitation frequency.

The typical field results of the flow velocity and pressure are presented in Figures 15–17. As shown in Figure 15, except the time when the piston changes its direction, the high-speed flow mainly occurs in the working gap due to the small ration of the gap width to the piston radius. The pressure in each chamber is nearly constant, with the large pressure gradient observed across

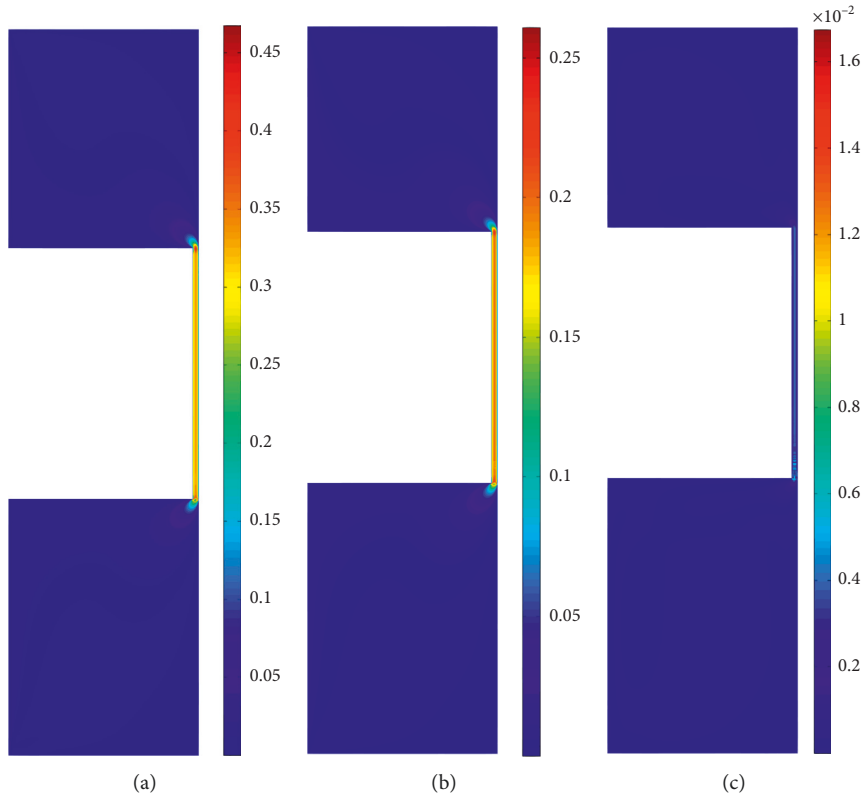

Figure 15: Magnitude of flow velocity (m/s) in the MR damper under sinusoidal displacement excitations of 1.27 cm, 0.2 Hz, 2 A: (a) $t = T/12$; (b) $t = 2T/12$; (c) $t = 3T/12$.

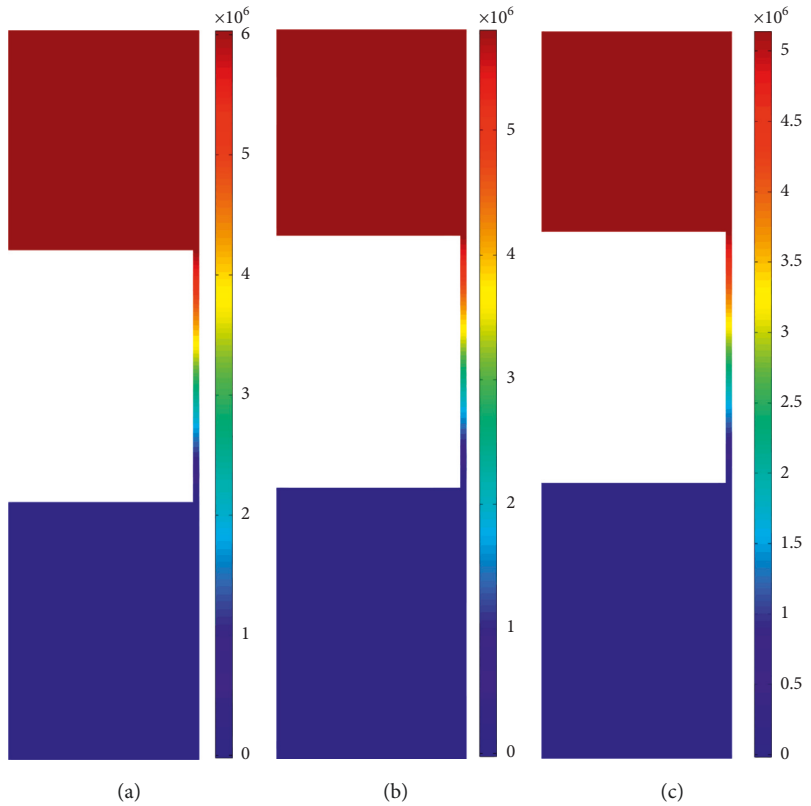

Figure 16: Pressure field (Pa) in the MR damper under sinusoidal displacement excitations of 1.27 cm, 0.2 Hz, 2 A: (a) $t = T/12$; (b) $t = 2T/12$; (c) $t = 3T/12$.

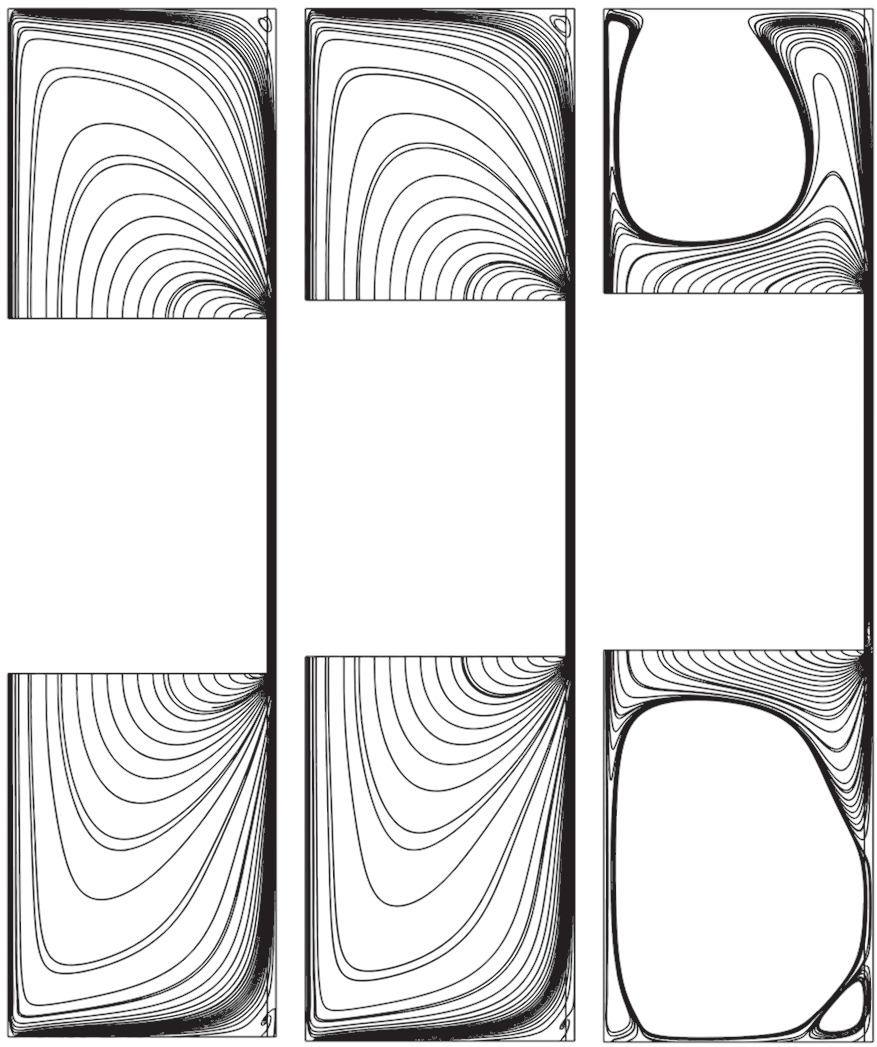

Figure 17: Stream lines within the MR damper under sinusoidal displacement excitations of 1.27 cm, 0.2 Hz, 2 A: (a) $t = T/12$; (b) $t = 2T/12$; (c) $t = 3T/12$.

the working gap (Figure 16). Moreover, the flow pattern can be more clearly seen from the steam lines in Figure 17, and large vortexes are observed when the piston reverses its direction ($t = T/4$).

5. Conclusions

This paper develops a two-dimensional axisymmetric finite element model for simulating the dynamic behavior of MR dampers. By describing the MR fluid as a viscoelastic material, the model successfully captures the hysteresis in the damping force with respect to the piston velocity. The solution of the model shows a slight mesh sensitivity. Except the time when the piston changes its direction, the high-speed flow occurs in the working gap due to the small ratio of the gap width to the piston radius. Large vortexes are generated in the chambers of MR dampers during the piston reversing its direction. The hysteresis of the damping force with respect to the piston velocity is frequency-dependent, and it becomes apparently wider with increasing excitation frequency.

Data Availability

All data generated or analyzed during this study are included in this paper.

Conflicts of Interest

The authors declare that they have no conflicts of interest.

Acknowledgments

This research was supported by the National Natural Science Foundation of China (no. 51308450), Foundation of Key Laboratory of Structures Dynamic Behavior and Control (Ministry of Education) in Harbin Institute of Technology (HITCE201708), and Research Foundation of Xi'an University of Architecture and Technology (no. RC1368).

References

[1] S. J. Dyke, B. F. Spencer, M. K. Sain, and J. D. Carlson, "Modeling and control of magnetorheological dampers for seismic response reduction," *Smart Materials and Structures*, vol. 5, no. 5, pp. 565–575, 1996.

[2] M.-G. Yang and C. S. Cai, "Longitudinal vibration control for a suspension bridge subjected to vehicle braking forces and earthquake excitations based on magnetorheological dampers," *Journal of Vibration and Control*, vol. 22, no. 17, pp. 3659–3678, 2016.

[3] N. Caterino, "Semi-active control of a wind turbine via magnetorheological dampers," *Journal of Sound and Vibration*, vol. 345, pp. 1–17, 2015.

[4] F. Gordaninejad and S. P. Kelso, "Fail-safe magneto-rheological fluid dampers for off-highway, high-payload vehicles," *Journal of Intelligent Materials Systems and Structures*, vol. 11, no. 5, pp. 395–406, 2000.

[5] D. X. Phu, S.-B. Choi, Y.-S. Lee, and M.-S. Han, "Vibration control of a vehicle's seat suspension featuring a magneto-rheological damper based on a new adaptive fuzzy sliding-mode controller," *Proceedings of the Institution of Mechanical Engineers, Part D: Journal of Automobile Engineering*, vol. 230, no. 4, pp. 437–458, 2016.

[6] Y.-T. Choi and N. M. Wereley, "Vibration control of a landing gear system featuring electrorheological/magnetorheological fluids," *Journal of Aircraft*, vol. 40, no. 3, pp. 432–439, 2003.

[7] D. C. Batterbee, N. D. Sims, R. Stanway, and Z. Wolejsza, "Magnetorheological landing gear: 1. A design methodology," *Smart Materials and Structures*, vol. 16, no. 6, pp. 2429–2440, 2007.

[8] D. C. Batterbee, N. D. Sims, R. Stanway, and M. Rennison, "Magnetorheological landing gear: 2. Validation using experimental data," *Smart Materials and Structures*, vol. 16, no. 6, pp. 2441–2452, 2007.

[9] İ. Şahin, T. Engin, and Ş. Çeşmeci, "Comparison of some existing parametric models for magnetorheological fluid dampers," *Smart Materials and Structures*, vol. 19, no. 3, article 035012, 2010.

[10] B. F. Spencer, S. J. Dyke, M. K. Sain, and J. D. Carlson, "Phenomenological model for magnetorheological dampers," *Journal of Engineering Mechanics*, vol. 123, no. 3, pp. 230–238, 1997.

[11] D. Wang and W. H. Liao, "Magnetorheological fluid dampers: a review of parametric modelling," *Smart Materials and Structures*, vol. 20, no. 2, article 023001, 2011.

[12] C. M. D. Wilson and M. M. Abdullah, "Structural vibration reduction using fuzzy control of magnetorheological dampers," in *Proceedings of the 2005 Structures Congress on Forensic Engineering Symposium*, New York, NY, USA, April 2005.

[13] R. M. Bhatnagar, "Transient effect modelling of magneto-rheological fluid–based damper at low speed and its comparison with the existing magnetorheological damper models," *Journal of Intelligent Material Systems and Structures*, vol. 24, no. 12, pp. 1506–1523, 2013.

[14] K. Esteki, A. Bagchi, and R. Sedaghati, "Dynamic analysis of electro-and magneto-rheological fluid dampers using duct flow models," *Smart Materials and Structures*, vol. 23, no. 3, article 035016, 2014.

[15] P. Guo, X. Guan, and J. Ou, "Physical modeling and design method of the hysteretic behavior of magnetorheological dampers," *Journal of Intelligent Material Systems and Structures*, vol. 25, no. 6, pp. 680–696, 2013.

[16] Q.-H. Nguyen and S.-B. Choi, "Dynamic modeling of an electrorheological damper considering the unsteady behavior of electrorheological fluid flow," *Smart Materials and Structures*, vol. 18, no. 5, article 055016, 2009.

[17] Q.-H. Nguyen and S.-B. Choi, "A new approach for dynamic modeling of an electrorheological damper using a lumped parameter method," *Smart Materials and Structures*, vol. 18, no. 11, article 115020, 2009.

[18] X. Wang and F. Gordaninejad, "Flow analysis and modeling of field-controllable, electro- and magneto-rheological fluid dampers," *Journal of Applied Mechanics*, vol. 74, no. 1, pp. 13–22, 2007.

[19] N. M. Wereley, L. Pang, and G. M. Kamath, "Idealized hysteresis modeling of electrorheological and magneto-rheological dampers," *Journal of Intelligent Material Systems and Structures*, vol. 9, no. 8, pp. 642–649, 1998.

[20] G. M. Kamath and N. M. Werely, "Nonlinear viscoelastic-plastic mechanisms-based model of an electrorheological damper," *Journal of Guidance, Control, and Dynamics*, vol. 20, no. 6, pp. 1125–1132, 1997.

[21] M. Yu et al., "Unsteady analysis for oscillatory flow of magnetorheological fluid dampers based on Bingham plastic and Herschel–Bulkley models," *Journal of Intelligent Material Systems and Structures*, vol. 24, no. 9, pp. 1067–1078, 2013.

[22] J. Zheng, Y. Li, Z. Li, and J. Wang, "Transient multi-physics analysis of a magnetorheological shock absorber with the inverse Jiles-Atherton hysteresis model," *Smart Materials and Structures*, vol. 24, no. 10, article 105024, 2015.

[23] A. Ursescu, *Channel Flow of Electrorheological Fluids under an Inhomogeneous Electric Field*, Technische Universität Darmstadt, Darmstadt, Germany, 2005.

[24] H. Sahin, X. Wang, and F. Gordaninejad, "Magneto-rheological fluid flow through complex valve geometries," *International Journal of Vehicle Design*, vol. 63, no. 2-3, pp. 241–255, 2013.

[25] H. Zhou and M. Bai, "Three-dimensional numerical simulation of magnetorheological fluid seal technology applied on circular cooler and its experimental validation," *Mechanics of Advanced Materials and Structures*, vol. 21, no. 4, pp. 329–340, 2014.

[26] J. Gołdasz and B. Sapiński, "Application of CFD to modeling of squeeze mode magnetorheological dampers," *Acta Mechanica et Automatica*, vol. 9, no. 3, pp. 129–134, 2015.

[27] A. Syrakos, Y. Dimakopoulos, G. C. Georgiou, and J. Tsamopoulos, "Viscoplastic flow in an extrusion damper," *Journal of Non-Newtonian Fluid Mechanics*, vol. 232, pp. 102–124, 2016.

[28] N. Caterino, M. Spizzuoco, and A. Occhiuzzi, "Understanding and modelling the physical behaviour of magnetorheological dampers for seismic structural control," *Smart Materials and Structures*, vol. 20, no. 6, article 065013, 2011.

[29] N. Caterino, M. Spizzuoco, and A. Occhiuzzi, "Promptness and dissipative capacity of MR dampers: experimental investigations," *Structural Control and Health Monitoring*, vol. 20, no. 12, pp. 1424–1440, 2013.

[30] D. Case, B. Taheri, and E. Richer, "Multiphysics modeling of magnetorheological dampers," *International Journal of Multiphysics*, vol. 7, no. 1, pp. 61–76, 2013.

[31] A. Sternberg, R. Zemp, and J. C. de la Llera, "Multiphysics behavior of a magneto-rheological damper and experimental validation," *Engineering Structures*, vol. 69, pp. 194–205, 2014.

[32] M. Behr, D. Arora, O. M. Coronado, and M. Pasquali, "GLS-type finite element methods for viscoelastic fluid flow simulation," in *Proceedings of the Third MIT Conference on*

*Computational Fluid and Solid Mechanics*Massachusetts Institute of Technology, Cambridge, MA, USA, 2005.

[33] R. B. Bird, R. C. Armstrong, and O. Hassager, *Dynamics of Polymeric Liquids: Fluid Mechanics*, Wiley, Vol. 1, Hoboken, NJ, USA, 1987.

[34] G. Yang, *Large-Scale Magnetorheological Fluid Damper for Vibration Mitigation: Modeling, Testing and Control*, University of Notre Dame, Notre Dame, IN, USA, 2001.